Geo-Mar Lett (2002) 22: 133–141
DOI 10.1007/s00367-002-0104-z

G. Guerin · D. Goldberg

Heave compensation and formation strength evaluation from downhole acceleration measurements while coring

Received: 19 December 2001 / Accepted: 10 June 2002 / Published online: 31 July 2002
© Springer-Verlag 2002

Abstract In order to evaluate the efficiency of heave compensation in the Ocean Drilling Program, we developed a device measuring the acceleration of the core barrels. First results show that heave compensation limits bit motion to 10% of the surface heave. We also use the acceleration data to characterize the formation. On rotary corers, acceleration amplitudes decrease with increasing hardness of the formation. Comparison with geophysical logs shows that this relationship can resolve cm-scale features. On piston corers, the maximum acceleration is characteristic of the sediment shear strength. Easy and fast to deploy, this tool allows to characterize formations before any sample analysis.

Introduction

Accurate depth control has always been one of the primary concerns of the Ocean Drilling Program (ODP). In water depths typically ranging between 500 and 6,000 m, the problem is particularly acute during cruises which rely on recovering cm-scale features such as thin sediment bedding, ash horizons, or hard grounds in slow sedimentation environments. The identification of the seafloor itself, when covered with soft sediments, is also rarely unequivocal. In the absence of a clear reference datum, monitoring of the seafloor penetration and of specific horizons has relied on empirical methods such as multiple coring. The inherent difficulty in recovering drill cores as far as 8 km below the sea surface from a floating ship entails significant uncertainties in the operations. Heave compensation systems have been designed to reduce this uncertainty. Controlled by onboard instrumentation which monitors the movement of the ship, the top-drive (rotating table) is mounted on vertical rails along the derrick which allows hydraulic cylinders to adjust its vertical motion for ship heave. However, in the usual range of operating depths for ODP, the stretching and oscillations of the 9-inch-diameter drill string can be significant, and the actual motion of the drill bit is mostly unknown.

To evaluate the efficiency of the heave compensation, a device was designed by the Borehole Research Group at Lamont-Doherty Earth Observatory to measure acceleration on various coring tools used in the Ocean Drilling Program. The drill string acceleration tool (DSA) is a memory probe recording pressure and three-component acceleration attached on the top of the core barrel. The true vertical displacement at the bit cannot be measured directly, but it can be integrated from the acceleration data.

In this paper, we describe the specifications of the DSA, its mode of operation, and we present the first data recorded during ODP legs 185 and 191. Both locations were drilled in similar settings on the northwest Pacific plate, into Neogene to Cretaceous siliceous clay and oozes overlaying chert-rich calcareous oozes or chalk which were deposited on the Cretaceous/Jurassic basement (Plank et al. 2000; Kanazawa et al. 2001). We estimate vertical displacement at site 1149 to evaluate the efficiency of the heave compensation. We compare data recorded in different coring environments to show how the DSA records are sensitive to the nature and induration of the formation. We interpret the rotary coring acceleration data using spectral analysis and comparison of time records with formation properties derived from well logs. Finally, we use DSA records from piston coring to estimate formation shear strength.

Materials and methods

Specifications

The principal components of the DSA are a pressure sensor and two accelerometers. The pressure sensor

G. Guerin (✉) · D. Goldberg
Borehole Research Group, Lamont-Doherty Earth Observatory,
Rte 9 W, P.O. Box 1000, Palisades, NY 10964, USA
E-mail: guerin@ldeo.columbia.edu
Tel.: +1-845-3658671
Fax: +1-845-365 3182

measures pressure in the drill pipe every second, which is used to trigger the recording of acceleration data at a pre-programmed depth. One accelerometer is a vertical-component high-sensitivity transducer, recording motion along the axis of the drill string. The other is a high-frequency three-axis transducer to record bit vibrations. The DSA runs as a self-contained memory device with a battery life allowing 9 h of operations and enough memory to record about 1.5 h of data at a 100-Hz sampling frequency. Before deployment, the DSA is connected through a serial port to a data acquisition PC for initialization, and the initial recording depth is defined, typically 100 m above coring depth. After recovery, the DSA is reconnected to the PC and the data are downloaded as Ascii files ready for immediate analysis. The first processing step is the conversion of the raw data into acceleration, using calibration coefficients provided by the accelerometer manufacturers. The sensors, electronics board, memory and batteries are enclosed in a 1.2-m-long stainless steel pressure case (see Fig. 1) and can operate under temperature and pressure up to 85 °C and 75 MPa, respectively. Specifications are summarized in Table 1.

Operations

Continuous coring in ODP holes is performed by recovering the core barrel at regular intervals, typically every 9.5 m. The procedure is the same for advanced piston coring (APC) in soft sediments, and for the rotary coring bit (RCB) in harder formations. The empty core barrel free falls to the bottom of the drill string, advances 9.5 m during coring, and then is retrieved by a wireline which latches to the top of the core barrel. After reaching the rig floor, the core is removed for analysis and an empty core barrel is dropped in the drill string to continue the coring process.

The DSA was designed to minimize any impact on coring operations. The tool is initialized before a core barrel is prepared for descent. The DSA is then attached by threaded collars to the top of the core barrel (Fig. 1) and the DSA/core barrel assembly is let free falling to the bottom of the drill string. The top of the DSA can receive the normal core retrieval tool, and the entire assembly is recovered together. Only a few minutes are added to the normal rig floor operations to make and disassemble the DSA/core barrel connection. Before any core analysis is performed (cores must usually rest for a few hours to degas and reach thermal equilibrium), the DSA data are available to assess the coring process and characterize formation attributes.

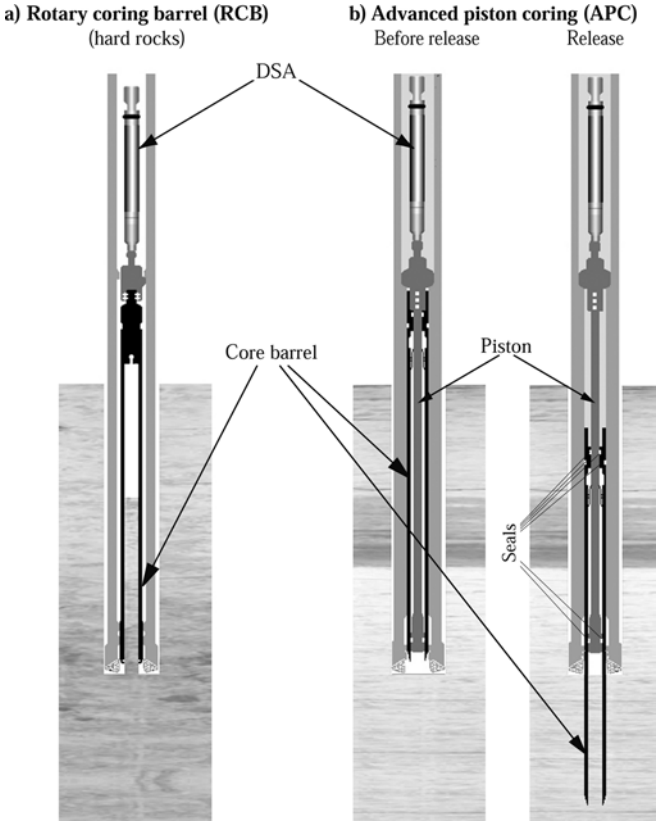

Fig. 1 Configuration of the DSA/core barrel assembly during **a** rotary coring, and **b** piston coring. In **b**, we show the assembly before and after the core barrel has been pushed into the formation

Results

DSA acceleration data

Figure 2 shows typical DSA acceleration data recorded with APC (Fig. 2a) and RCB (Fig. 2b) during leg 185 near the Izu-Bonin trench. The pressure increase at the beginning of each record corresponds to the end of the free fall of the core barrel. In the APC record (Fig. 2a), additional time is spent to ensure that the core barrel has actually reached the bottom. At ~600 s, the pressure is raised in the pipe to a threshold which releases the piston to penetrate ahead of the bit. The total pressure increase is actually about 3,000 psi (20 MPa) but the pressure

Table 1 Specifications of the DSA

Parameter	Value
Weight	34 kg
Length	1.20 m
Acceleration range one-axis sensor	–2, +2 g (=–19.62, 19.62 m s^{-2})
Acceleration range three-axis sensor	–4, +4 g (=–39.24, 39.24 m s^{-2})
Acceleration sampling rate	100 Hz
Acceleration precision one-axis sensor	4×10^{-3} g (=3.9×10^{-2} m s^{-2})
Acceleration precision three-axis sensor	8×10^{-3} g (=7.8×10^{-2} m s^{-2})
Raw data storage	16 bit integers
Total data storage	4 Mb (~90 min)
Pressure sampling rate	1 Hz
Pressure measurement range	0–75 MPa
Pressure resolution	1 psi (=7×10^{-3} MPa)
Power source	6 "AA" batteries (9.0 V)

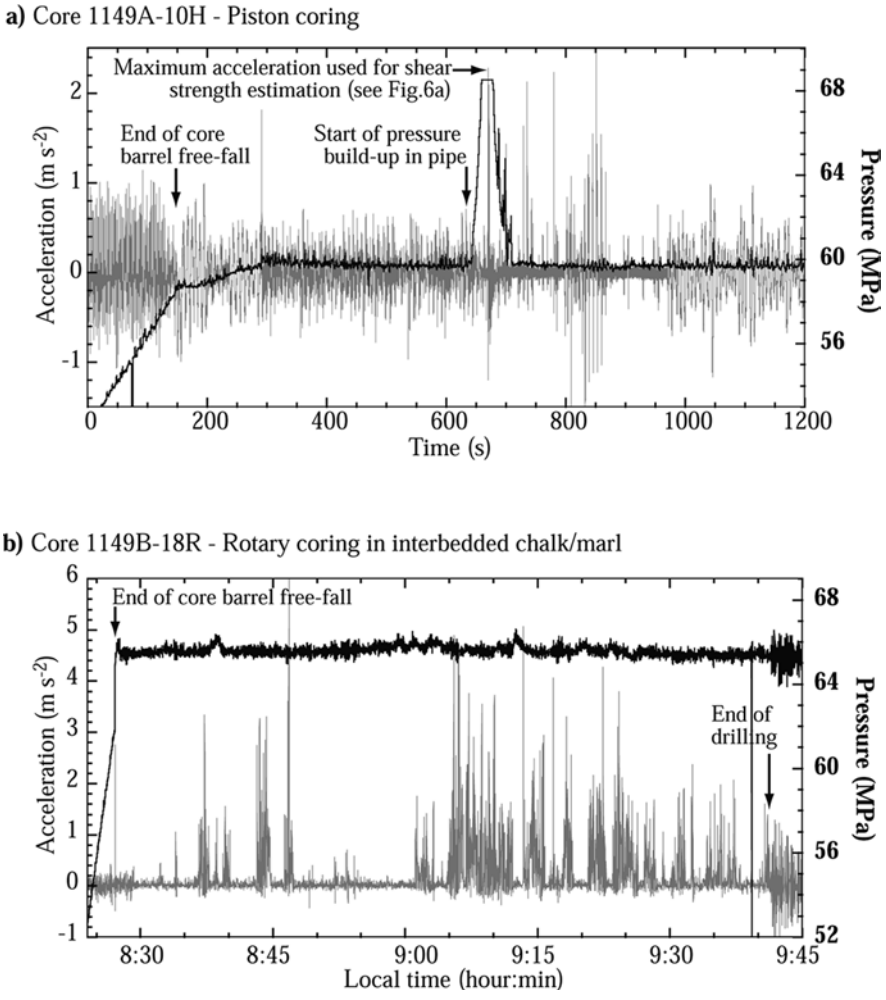

Fig. 2 Examples of DSA data recorded during **a** piston coring, and **b** rotary coring. Acceleration is in light *shading*, pressure in dark. The uniform gravity field has been subtracted from the acceleration data

sensor is saturated at ~68.5 MPa. The multiple spikes in the pressure curve during the pressure release correspond to the reflection of the initial pressure pulse from the sea surface (the 12-km roundtrip takes about 8 s). The maximum acceleration is recorded immediately after the pressure release.

In the RCB record (Fig. 2b), the acceleration shows strong variations over time without any change in coring operations. When drilling ceases and the heave compensation is stopped (at ~9:42), the signal/noise ratio of the acceleration and pressure records increases sharply. Our data show that transverse vibration records are similar to the longitudinal (*z*-axis) acceleration, albeit with lower amplitude, and that the two vertical accelerometers produce nearly identical records. Therefore, we limit the following analysis and discussion to the data recorded using the high-sensitivity vertical-axis transducer.

Heave compensation evaluation

To evaluate the efficiency of the heave compensation, we use the vertical acceleration data to calculate the vertical displacement of the core barrel. The tight coupling of the core barrel with the bottom hole assembly (BHA) assures that the vertical displacements of the DSA and of the drill bit are similar. We use the later portion of the DSA record from core 149B-18R (Fig. 2b) to calculate the vertical displacement at the bit before and after heave compensation stops. This record is the only one available in which drilling stops before the DSA recording. Hence, it is the only record for which evaluation of the heave compensation is feasible.

Before integrating the acceleration record twice over time, the static gravity acceleration ($g = 9.8067$ m s^{-2}) was subtracted from the acceleration data, and a 0.01–3 Hz band-pass filter was applied to remove high frequencies related to drill bit vibrations. This isolates the heave-related motion. The calculated displacement is compared with surface heave data in Fig. 3a. Once drilling and heave compensation stop, the drill bit vertical motion mirrors the surface heave (~1.5-m amplitude) whereas the displacement amplitude during drilling is about an order of magnitude lower (~15 cm). The filtering used in the displacement calculation eliminates the downward movement of the bit and the "zero" should be interpreted as a median bit position.

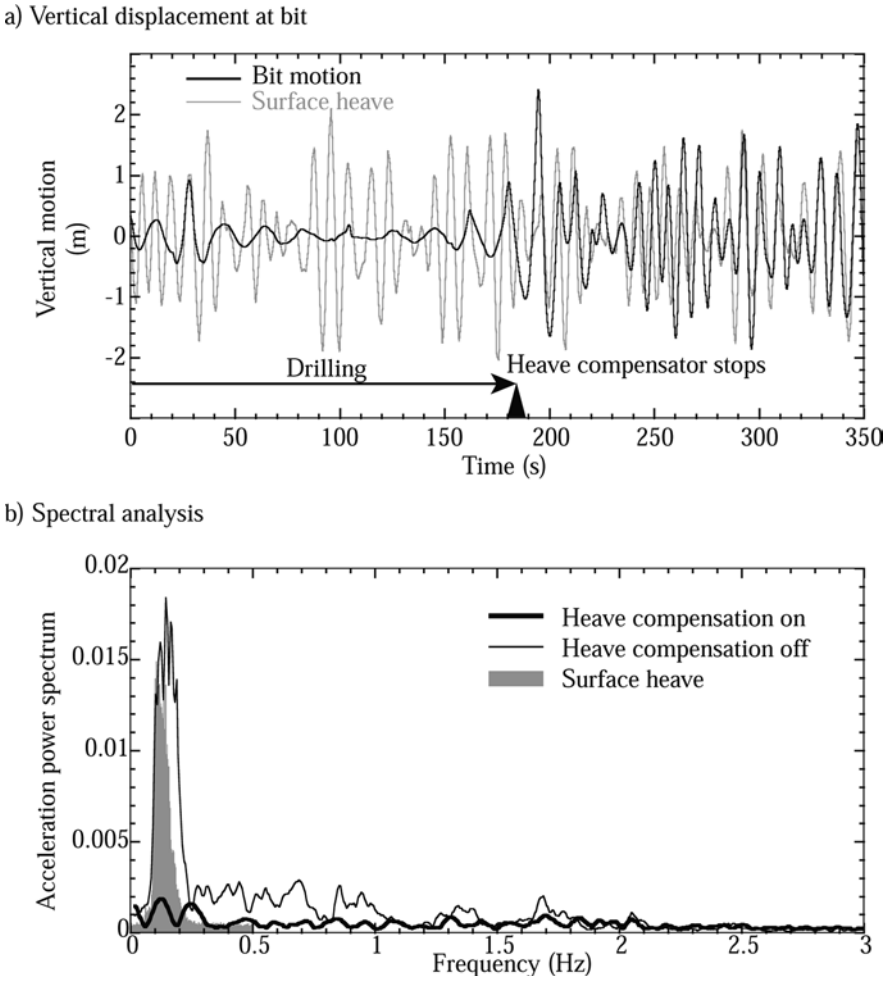

Fig. 3a, b Evaluation of the drilling heave compensation. **a** The displacement calculated by double integration of the acceleration shows that the amplitude of vertical motion at the bit is about 10% of the surface heave amplitude. The "negative" displacement of the bit is an artifact resulting from the filter removing the actual downward movement of the bit. The *0* corresponds to the median bit position. **b** Fast Fourier transform of the DSA with and without heave compensation. The surface heave spectrum is shown for comparison

A more general assessment of the heave compensation efficiency can be achieved using spectral analysis. Such analysis avoids the effects of noise on displacement integration and numerical approximations due to filtering. Figure 3b shows the fast Fourier transform of acceleration data with and without heave compensation, as well as the surface heave spectrum. This comparison shows that heave dominates the acceleration spectrum at the bit without compensation. It confirms also, as shown in the displacement analysis above, that compensation reduces the heave influence by about one order of magnitude. Heave compensation appears to be effective for frequencies up to 1 Hz, which corresponds to the drilling rotation rate. Higher frequency components of the acceleration spectrum do not appear to be affected by the heave compensation.

Lithology characterization

In Fig. 2b, the RCB acceleration data show significant amplitude changes with time, although drilling parameters were constant while recovering this core. This suggests that the RCB acceleration is dependent on the nature and/or induration of the formation. Core 1149B-18R penetrated chalks and interbedded chalk/marl in this interval (Plank et al. 2000). The notable variations in acceleration data in this record prompted comparison with records in other formations (from clays to basalt) which were drilled during leg 185. In a related experiment conducted during leg 179, Myers et al. (1999) explore the relationship between drill string acceleration amplitude and formation properties measured at the rig floor. In examples of poor core recovery, such relationships were shown to provide an estimate of the properties of the formation being drilled.

Figure 4 shows the spectra of the acceleration recorded in various types of formation encountered in four cores at site 1149. Fast Fourier transforms were all computed over 2^{17} samples or about 20 min of drilling data in each core. In the sedimentary cores (1149B-8R and -18R), the lithology is finely layered with interbedded hard chert and soft sediments, making core recovery difficult. Recovery rates were relatively poor (maximum 30% for core 1149B-30R; minimum 1% for core 1149B-8R), and the nature of the formation was often identified only by using log data (Plank et al. 2000).

At frequencies below ~2 Hz, which corresponds to frequencies close to the bit rotation rate, amplitudes become increasingly lower in harder formations: the

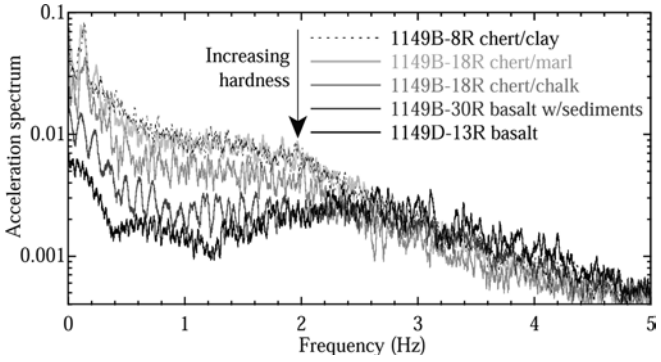

Fig. 4 Comparison of DSA record spectra in different types of formation. The amplitude generally decreases with increasing hardness of the formation

interbedded chert/clay and chert/marl (cores 1149B-8R and -18R) have the highest amplitude, the chert/chalks (core 1149B-18 R) are intermediate, and the basalt has the lowest amplitudes (cores 1149B-30R and 1149D-13R). Some fracture filling and interpillow sediments in core 1149B-30R generate slightly higher amplitudes than in the fresher basalt in core 1149D-13R. Acceleration spectra above ~2 Hz appear to be independent of the nature of the formation.

A finer-scale analysis of the time-domain acceleration data may also be used for correlation with core and well data. Figure 5 illustrates the correlation between the acceleration record, the natural gamma ray and resistivity logs, and the formation micro scanner (FMS) images for core 1149B-18R. FMS images are high-resolution microresistivity images of the formation recorded with four arms pushed against the borehole wall. At the end of each arm in contact with the formation, 16 "buttons" allow a sampling rate of 2.5 mm and a vertical resolution of 5 mm (Schlumberger 1989). Bright colors show hard, resistive features and dark colors show conductive layers and cracks. In Fig. 5, bright color bands correspond to chert layers. Because the penetration rate was not exactly uniform throughout this interval, we can not expect to observe a perfect depth-time match between the logs and DSA data sets, although both represent a complete record over this interval. In comparison, the core recovery rate was only 11% (~1.2 m of core recovered), and it comprised radiolarian marlstone, chert and porcellanite which are typically difficult to recover. The core recovered represents the harder layers which were penetrated; softer intervals are washed away during drilling. The actual depth of the samples within the cored interval is unknown and the core is placed arbitrarily at the top of the interval. Above ~306.5 m b.s.f., gamma ray and resistivity logs are generally high and DSA acceleration amplitude is generally low. The peak in the resistivity log at ~306.5 m b.s.f., also prominent as a bright band in the FMS image, corresponds to low acceleration between 9:02 and 9:05. Below 306.5 m b.s.f., low gamma ray and resistivity logs indicate increased marl content and correlate with generally higher acceleration. Intervals with low acceleration are associated with thin, resistive cherts and appear as bright bands in the FMS images. We indicate on the figure possible correlations between the FMS images and the DSA record. Such correlations could allow for a first-order estimate of formation properties in low-recovery environments.

Formation shear strength

During piston coring, the brevity of the operation (a few seconds for a 9.5-m core) precludes a time-series analysis

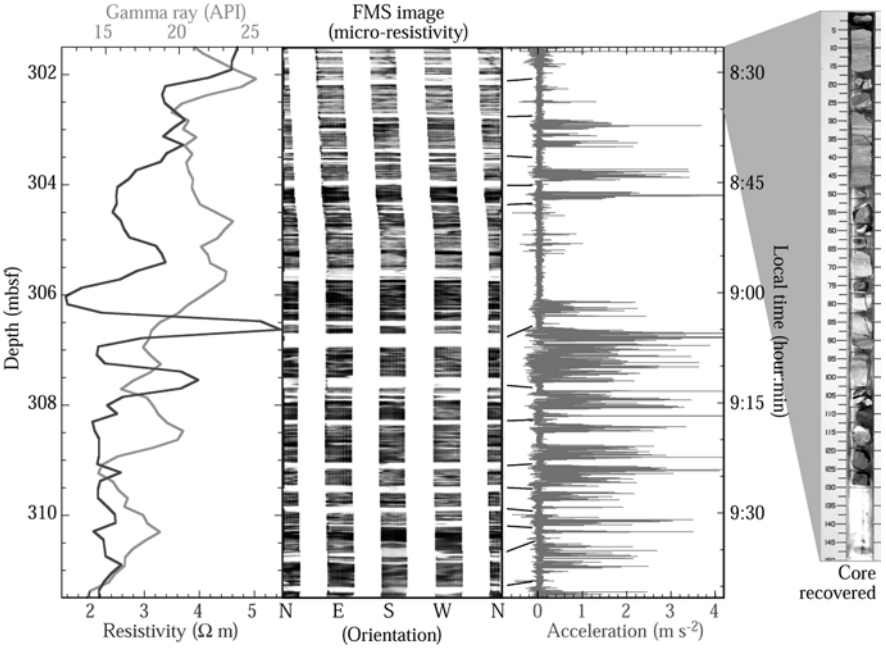

Fig. 5 Comparison of downhole logs (gamma ray in *light shade*, resistivity in *dark*), and FMS electrical images with the DSA record for core 1149B-18R. The logs are depth-referenced whereas the DSA is recorded as a function of time, preventing a perfect match of the records. We indicate possible correlations between resistive chert layers (*light shading* in the FMS images) and low-acceleration intervals. The recovery for this core was about 11%, and included only the hardest cherts and chalks of this finely layered formation

of DSA acceleration records. Because the DSA is designed to fit on top of the APC core barrel which acts like a penetrometer, it may nevertheless be used to estimate in-situ the undrained shear strength of the formation. Figure 6 suggests that the first peak in the acceleration record is characteristic of the initial penetration into the formation, as a reaction to the deceleration of the barrel entering the formation. Because of the location of the DSA at the top of the piston, however, any quantification requires that the dynamic coupling between the piston and the core barrel be taken into account. We assume that this coupling can be defined by a simple damping coefficient η between the piston, the barrel, the BHA and the intermediate seals. The equations of the piston and barrel movements are developed in the Appendix. The derived expression for the force of the formation on the core barrel is

$$F_{\text{formation}} = a_o\left(m_{\text{barrel}} + 2m_{\text{piston}}\right) - m_{\text{barrel}}\pi r_{\text{piston}}^2\eta^{-1}dP/dt + (P_o - P)\pi\left(r_{\text{barrel}}^2 + r_{\text{piston}}^2\right) + \eta v_{\text{piston}} \quad (1)$$

where m_{piston}, m_{barrel}, r_{piston}, and r_{barrel} are the mass and radii of the piston and core barrel, P_o is the hydrostatic pressure, P is the pressure in the pipe measured by the DSA, dP/dt is its time derivative, and v_{piston} is the velocity of the piston/DSA assembly. All these values are measured at the time of maximum acceleration and can be derived or measured from the data recorded by the DSA. Assuming that the piston sits rigidly on its landing support until impact, v_{piston} can be calculated by integration of a_o between the beginning of the movement and the peak acceleration.

$F_{formation}$ is directly related to the undrained shear strength of the formation, which is the value which we seek. Beard (1985) decomposes the reaction of the formation on a penetrometer into a bearing component and a side adhesion force, both functions of the formation shear strength. The resulting relationship between $F_{formation}$ and the undrained shear strength S_u is

$$F_{formation} = S_u S_e^* \frac{(N_c A_f + A_s/S_t)}{1 + \frac{1}{\sqrt{(C_e v_{barrel}/S_u t) + 0.6}}} \quad (2)$$

where N_c is the formation bearing capacity factor, t, A_f and A_s are the diameter, the frontal area and the side area of the cutting shoe, respectively, S_t is the sediment sensitivity, S_e^* and C_e are empirical strain rate coefficients, and v_{barrel} is the velocity of the cutting shoe. Using the value of $F_{formation}$ calculated with Eq. (1), and values for S_e^*, C_e, S_t and N_c given by Beard (1985) and Senneset and Janbu (1985), S_u can be deduced from Eq. (2) as the positive root of a third order polynomial (see Appendix).

Our estimates of S_u for the three DSA-APC records from legs 185 and 191 (sites 1149 and 1179, respectively) are summarized in Table 2. Because the DSA pressure sensor saturated on core 1149A-10H, we have used average values of P and dP/dt from the two other cores in computing $F_{formation}$ for this core. Drilling parameters and sub-seafloor depth are similar for these three cores, whereas the S_u value increases by almost a factor of two between siliceous clay (core 1149A-10H) and clay-bearing ooze (cores 1179C-4H and 1179C-7H). We compare these results with vane-shear strength measurements performed on laboratory samples from the same cores. The results from the shear vane test show much less contrast between the two sites. In addition to the difference in lithology, the discrepancy between the vane shear and DSA results also reflects distinct in-situ conditions. The greater water depth at site 1149 causes higher pore pressure in these sediments, although the overburden pressure of the overlying sediments is similar to that at site 1179. The resulting higher support from the pore fluid, which has no shear strength, reduces the in-situ formation shear strength. This is not reflected in the vane shear measurements.

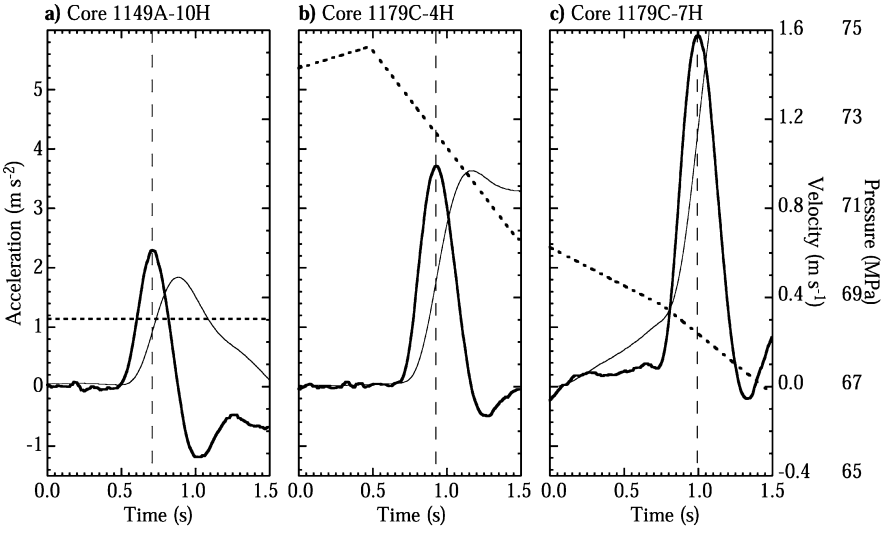

Fig. 6a–c DSA records for the three APC cores on which the DSA was deployed during ODP legs 185 and 191. **a** Core 1149A-10H, **b** core 1179C-4H, and **c** core 1179C-7H. *Continuous thick lines* are acceleration, *thin lines* are velocity, and *dotted lines* are pressure. The first peak in each acceleration record is characteristic of the formation being drilled. The pressure, acceleration and velocity used to calculate $F_{formation}$ in Eq. (9) are measured at the peak indicated by the vertical, *fine dashed lines*. The pressure sensor saturated during the deployment on core 1149A-10H

Table 2 Estimated shear strength in poorly consolidated sediments

Core	Depth (m b.s.f.)	Water depth (m)	Sediment type	Vane shear strength (kPa)	a_o (m s^2)	v_{piston} [b] (m s^{-1})	DSA shear strength (kPa)
1149A-10H	80	5,867	Siliceous clay	56–64[a]	2.4	0.2	274
1179C-4H	77	5,564	Clay-bearing ooze	40–61[a]	3.6	0.5	434
1179C-7H	105	5,564	Clay-bearing ooze	40–80[a]	5.9	1.1	457

[a]Shear vane measurements were made on several samples per core. These values represent the range of values measured

[b]v_{piston} is calculated by time-integration of a_o between the initial movement and the peak maximum

Discussion

Lee (1985) discusses the validity of various types of shear strength measurements and observes that the ratio of the results from in-situ penetrometer to laboratory vane shear strength measurements can be as high as 30, and that the ratio between in-situ shear vane and in-situ penetrometer values is on the order of 10. Each type of measurement can be used with confidence, but comparison between the various kinds of in-situ and laboratory data may be difficult because of systematic measurement biases. In particular, most laboratory measurements do not replicate in-situ conditions. Because some of the parameters used in Eq. (1) and in the Appendix are approximate (including the damping coefficient and the bearing capacity factor), our in-situ estimate may not represent accurate values for all conditions.

One possible improvement to the tool which would allow for a more accurate estimation of the shear strength would be to put the accelerometer inside the cutting shoe. This would eliminate the various approximations made for the piston/barrel dynamics. Some tools used routinely by the ODP have this type of configuration, such as the APC/Adara temperature probe in which the electronics, batteries and sensors are located in an annular cavity in the cutting shoe (Shipboard Scientific Party 1992). In addition, data recorded by sensors inside the cutting shoe can be used to integrate accurately the motion of the probe as it penetrates the formation (Villinger et al. 1999). In this configuration, $F_{formation}$ is directly related to the acceleration and pressure measured, and Eq. (2) can be used to draw a continuous shear strength profile.

In its present configuration, the DSA produces data which are indicative of the relative changes in formation properties during each coring operation. These data are sensitive to the formation shear strength under in-situ conditions but should be used with caution in comparison to shear vane measurements or other in-situ penetrometer data. Estimates of formation shear strength from DSA data are representative but future DSA deployments during piston coring would allow improvement of the approximations and assumptions made in this method. At this stage, perhaps the most useful applications of the DSA data to formation evaluation are the relative comparison between cores and the correlation of core and log data when recovery is poor.

Conclusions

This study presents the results from the first deployments of the DSA tool, allowing the efficiency of the drilling heave compensation to be evaluated quantitatively for the first time. We find that vertical bit motion is reduced by one order of magnitude compared to surface heave. Our results also show that this tool can be used to provide a fast characterization of formation properties. DSA data can help establish some of the properties of hard rocks being drilled with RCB coring, despite low recovery. The DSA may be used with APC core barrels to estimate in-situ the shear strength of the sediments. We recommend future deployments of the DSA in a variety of lithologic environments and under different drilling conditions to link physical properties of the core to coring operations.

Acknowledgements We thank Tom Pettigrew for providing us with information on the drilling technologies used in the ODP. H. Villinger's review contributed to the improvement of this manuscript.

Appendix

Derivation of formation reaction ($F_{formation}$) from DSA data

We assume that the DSA is rigidly assembled to the piston, so the acceleration measured (a) obeys the force balance equation for the piston:

$$m_{piston}a = m_{piston}g + F_{barrel/piston} + P_{pipe/piston} + R_{BHA} \quad (3)$$

where m_{piston} is the mass of the DSA/piston assembly, g is the gravity acceleration, $F_{barrel/piston}$ is the frictional force of the core barrel on the piston, $P_{pipe/piston}$ is the force of the fluid accumulated in the pipe, and R_{BHA} is the reaction of the pipe where the piston sits (see Fig. 7). We assume that once motion is detected, the piston/DSA assembly does not rest on its landing and that, consequently, R_{BHA} is null. The piston, barrel and bottom hole assembly are assumed to be perfectly aligned,

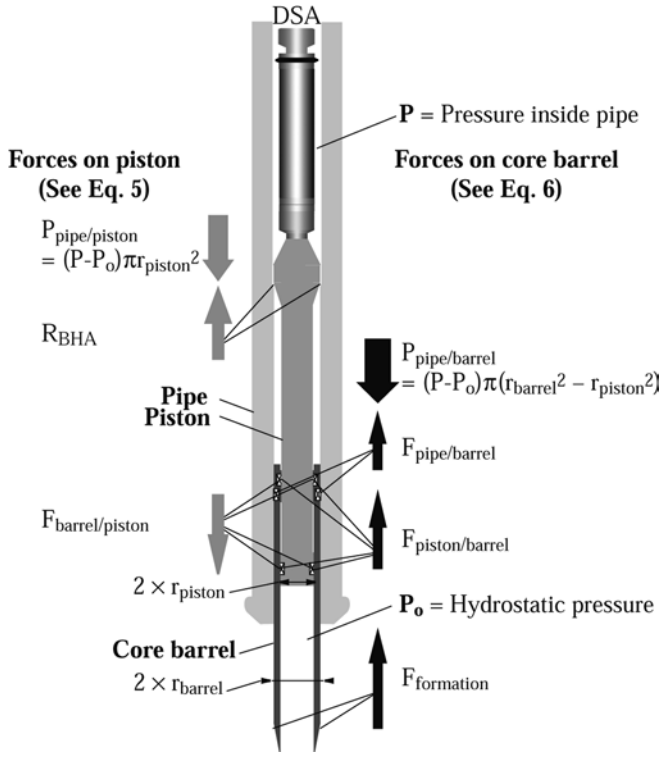

Fig. 7 Summary of the forces applied to the piston and to the core barrel. All friction forces between the core barrel, the piston and the pipe are assumed to be exerted through the different seals

and all motions and actions are one-dimensional along the pipe axis. Therefore, all equations are simply algebraic.

$P_{pipe/piston}$ is proportional to the pressure differential between the fluid in the pipe and hydrostatic pressure below the seals. The DSA pressure sensor measures the pressure P above the piston. The pressure record before buildup for APC initiation represents the hydrostatic pressure P_o. If r_{piston} is the radius of the piston rod, then

$$P_{pipe/piston} = (P - P_o)\pi r_{piston}^2 \tag{4}$$

We are interested in the reduced acceleration $a_o = a$–g which corresponds to the DSA motion. After subtracting the gravity field g, Eq. (3) can be rewritten

$$m_{piston} a_o = F_{barrel/piston} + (P - P_o)\pi r_{piston}^2 \tag{5}$$

A similar equation can be derived for the core barrel dynamics:

$$m_{barrel} a_{barrel} = F_{piston/barrel} + F_{pipe/barrel} + (P - P_o)\pi\left(r_{barrel}^2 - r_{piston}^2\right) + F_{formation} \tag{6}$$

where a_{barrel} is the reduced barrel acceleration, $F_{piston/barrel}$ ($=-F_{barrel/piston}$) and $F_{pipe/barrel}$ are the frictional forces against the piston and the inner pipe, respectively, r_{barrel} is the outer radius of the core barrel, $(P–P_o)\pi(r_{barrel}^2–r_{piston}^2)$ represents the driving action of the pipe fluids, and $F_{formation}$ is the reaction of the formation. We assume that the interaction between the core barrel and the piston, as well as that between the barrel and the drill pipe obey simple damping laws exerted through the various seals shown in Fig. 7. These friction forces are:

$$F_{barrel/piston} = \eta_{piston}\left(v_{barrel} - v_{piston}\right) \text{ and } F_{pipe/barrel} = -\eta_{BHA} v_{barrel} \tag{7}$$

where $v_{barrel}–v_{piston}$ is the relative speed of the barrel to the piston, and η_{piston} and η_{BHA} are the damping coefficients between the piston and the barrel, and the barrel and the BHA, respectively. These coefficients are characteristic of the building materials: for simplification, stainless steel for the piston, the core barrel and the BHA, and polyurethane for the seals. Because all seals are made from the same material and have the same dimensions, we assume that all metal surfaces are similar, and that the damping coefficient is the same η.

In this study, we pursue a simple indicator to estimate formation strength. The first peak in the acceleration record is characteristic of the initial penetration into the formation. The peak maximum corresponds to a null acceleration gradient: $da_o/dt = 0$. From Eqs. (5) and (7), this yields:

$$\eta(a_o - a_{barrel}) = \pi r_{piston}^2 dP/dt \text{ or } a_{barrel} = a_o - \pi r_{piston}^2/\eta dP/dt \tag{8}$$

Combining Eqs. (5), (6), (7) and (8), a relationship between recorded acceleration and formation strength is:

$$F_{formation} = a_o\left(m_{barrel} + 2m_{piston}\right) - m_{barrel}\pi r_{piston}^2/\eta dP/dt + (P_o - P)\pi\left(r_{barrel}^2 + r_{piston}^2\right) + \eta v_{piston} \tag{9}$$

where v_{piston} is the piston velocity when a_o is maximum.

Without an existing value for the damping coefficient, we have estimated a value from the beginning of the peak where $a_o = 0$ and $v_{piston} = 0$. In this case, Eqs. (5) and (9) give $F_{barrel/piston} = (P–P_o)\pi r_{piston}^2 = \eta v_{barrel}$, or $\eta = (P–P_o)\pi r_{piston}^2/v_{barrel}$. Assuming a value for v_{barrel} of 1.0 m s^{-1} shows that η is on the order of $1.0e^{+05}$ kg s^{-1}.

Formation shear strength from $F_{formation}$

Beard (1985) decomposes the reaction of the formation on a penetrometer into a bearing component force and a side adhesion force:

$$F_{formation} = S_e(S_u N_c A_f) + S_e(S_u A_s/S_t) \tag{10}$$

where S_e is the sediment strain rate factor, N_c is the bearing capacity factor, A_f and A_s are the frontal and side areas of the barrel, respectively, and S_t is the sediment sensitivity. S_u is the undrained shear strength of the

formation, which is the parameter of interest in this analysis. Beard (1985) gives values of sediment sensitivity (S_t) for different types of sediments, and we used the analysis of Senneset and Janbu (1985) to choose a bearing capacity factor (N_c) of 100.

The sediment strain rate can be related to the shear strength by

$$S_e = \frac{S_e^*}{1 + \frac{1}{\sqrt{(C_e v_{barrel}/S_u t) + 0.6}}} \quad (11)$$

where S_e^* is an empirical maximum strain rate factor ($S_e^* = 2$), C_e is an empirical strain rate coefficient ($C_e = 1{,}900$ Pa s), v_{barrel} is the velocity of the cutting shoe, and t is the cutting shoe diameter (Beard 1985). Eqs. (5) and (7) make it possible to express v_{barrel} from the measured data:

$$v_{\mathrm{barrel}} = v_{\mathrm{piston}} + \eta^{-1}\left(\mathrm{m_{piston}a_o} - (\mathrm{P} - \mathrm{P_o})\pi \mathrm{r_r^2}\right). \quad (12)$$

If we define $\alpha = S_e^* (N_c A_f + A_s/S_t)$ and $\beta = C_e v_{barrel} t^{-1}$, then Eqs. (10) and (11) can be combined to show that S_u is the positive root of a third-order polynomial:

$$0.6\alpha^2 \mathrm{S_u^3} + \alpha(\beta\alpha - 1.2\mathrm{F_{formation}})\mathrm{S_u^2} - \mathrm{F_{formation}}(2\alpha\beta + 0.4\mathrm{F_{formation}})\mathrm{S_u} + \beta F_{formation}^2 = 0. \quad (13)$$

The values used for the different parameters are summarized in Table 2.

References

Beard RM (1985) Expendable Doppler penetrometer for deep ocean sediments measurements. In: Strength testing of marine sediments: Laboratory and in-situ measurements. Am Soc Testing Mater Spec Tech Publ 883:101–124

Kanazawa T, Sager WW, Escutia C et al. (2001) Proceedings ODP, Initial Reports 191. http://www-odp.tamu.edu/publications/191_IR/191ir.htm

Lee HJ (1985) State of the art: Laboratory determination of the strength of marine soils. In: Strength testing of marine sediments: Laboratory and in-situ measurements. Am Soc Testing Mater Spec Tech Publ 883:181–250

Myers G, Goldberg D, Meltser A, Scholz E, ODP Leg 179 Scientific Party (1999) Petro-physical applications of new seismic-while-drilling technology in deep water. In: Proc 40th SPWLA Annual Logging Symp, Oslo, 30 May–3 June 1999, pap VV

Plank T, Ludden JN, Escutia C et al. (2000) Proceedings ODP, Initial Reports 185. http://www-odp.tamu.edu/publications/185_IR/185ir.htm

Schlumberger (1989) Log interpretation principles/applications. Schlumberger Educational Services, Houston, TX

Senneset K, Janbu N (1985) Shear strength parameters obtained from static cone penetration tests. In: Strength testing of marine sediments: Laboratory and in-situ measurements. Am Soc Testing Mater Spec Tech Publ 883:41–54

Shipboard Scientific Party (1992) Explanatory notes. In: Proceedings Ocean Drilling Program. Texas A&M University, College Station, TX, Init Rep 139, pp 55–95

Villinger H, Grigel J, Heesemann B (1999) Acceleration-monitored coring revisited. Geo-Mar Lett 19:275–281